Chemical Engineering Journal 111 (2005) 119–134

Chemical Engineering Journal

www.elsevier.com/locate/cej

Mathematical model and numerical simulation of the dynamics of flocculated suspensions in clarifier–thickeners

Raimund Bürger [a,*], Kenneth H. Karlsen [b], John D. Towers [c]

[a] *Institute of Applied Analysis and Numerical Simulation, University of Stuttgart, Pfaffenwaldring 57, D-70569 Stuttgart, Germany*
[b] *Centre of Mathematics for Applications (CMA), University of Oslo, P.O. Box 1053, Blindern, N-0316 Oslo, Norway*
[c] *MiraCosta College, 3333 Manchester Avenue, Cardiff-by-the-Sea, CA 92007-1516, USA*

Abstract

We formulate a mathematical model for continuous sedimentation–consolidation processes of flocculated suspensions in clarifier–thickener units. The governing equation of this model is a scalar, strongly degenerate parabolic equation in which both the convective flux and the diffusion term depend on parameters that are discontinuous functions of the depth variable. A simple finite-difference scheme for the numerical solution of the model is introduced. We perform a limited analysis of steady states as desired stationary modes of operation. Finally, numerical examples illustrate that the model realistically describes the dynamics of flocculated suspensions in clarifier–thickeners.

Keywords: Clarifier–thickener units; Discontinuous flux; Degenerate diffusion; Uniqueness; Stationary solutions; Finite-difference scheme; Numerical simulation

1. Introduction

Continuously operated clarifier–thickener units for the solid–liquid separation of suspensions were invented in 1905 by Dorr [1] and are now widely used in chemical engineering, mineral processing, the pulp-and-paper and food industries and wastewater treatment. Early attempts to model mathematically the operation of these units were made soon after their invention, see for example [2,3] and, for extended historical discussions, the review papers [4–6]. A mathematically rigorous framework, however, was established only very recently, and is based on a thorough investigation of nonstandard convection–diffusion equations with discontinuous and degenerating coefficients.

For many purposes, spatially one-dimensional mathematical models of these units are sufficient. These models are usually based on the well-known kinematic sedimentation theory by Kynch [7], which describes the batch settling of an ideal suspension of small, equal-sized rigid spheres in a viscous fluid by the conservation law

$$\frac{\partial u}{\partial t} + \frac{\partial b(u)}{\partial x} = 0$$

for the solids volume fraction u as a function of depth x and time t. The material specific properties of the suspension under study are described by the Kynch batch flux density function $b(u)$. If a global conservation of mass principle is taken into account, then the extension of this theory to clarifier–thickener units leads to a conservation law with a flux that depends discontinuously on x. This discontinuity is due to the split of the suspension feed flow into upwards- and downwards-directed bulk flows into the clarification and thickening zones, respectively. The discontinuous flux forms a challenge for the well-posedness analysis and the design of robust simulation tools for the clarifier–thickener model that have been resolved only very recently [8–14].

As is well known, the solution of the conservation law arising from the kinematic theory propagates along characteristics, which are straight lines in cylindrical vessels. (Due to the intersection of characteristics, solutions become in general discontinuous.) However, most suspensions are

* Corresponding author. Present address: Departmento de Ingeniería Matemática, Universidad de Concepción, Casilla 160-C, Concepción, Chile. Tel.: +49 711 6857647; fax: +49 711 6855599.
E-mail addresses: buerger@mathematik.uni-stuttgart.de (R. Bürger), kennethk@math.uio.no (K.H. Karlsen), jtowers@cts.com (J.D. Towers).

1385-8947/$ – see front matter © 2005 Elsevier B.V. All rights reserved.
doi:10.1016/j.cej.2005.02.007

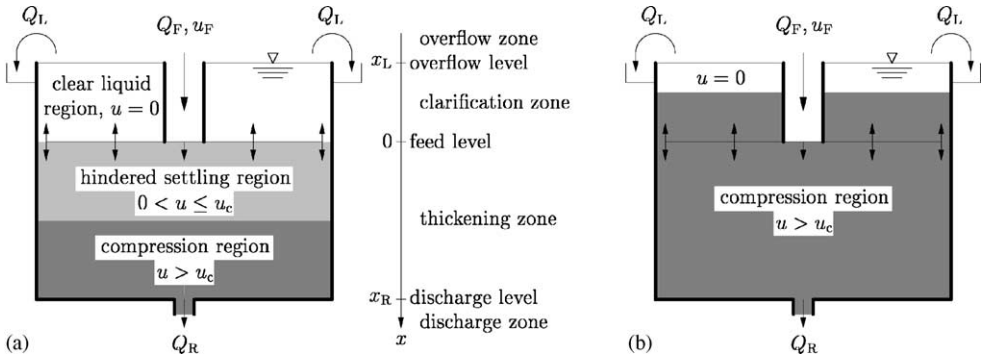

Fig. 1. A clarifier–thickener unit treating a flocculated suspension: (a) steady-state operation in conventional mode; (b) steady-state operation in high-rate mode.

not ideal; rather, they consist of small flocs, or are *flocculated*. These mixtures include inorganic slurries such as tailings from mineral processing, which are flocculated artificially in order to enhance settling rates, as well as biological sludges in wastewater treatment. They form compressible sediment layers, which are characterized by curved iso-concentration lines in cylindrical settling columns, and can therefore not be predicted by the kinematic theory. Instead, an extended dynamic model including pore pressure and effective solids stress has to be used. Such a model is provided by a theory of sedimentation–consolidation processes outlined in [15–17]. In one space dimension, the governing sedimentation–consolidation equation is a quasilinear degenerate parabolic equation, which degenerates into the equation of first-order hyperbolic type of the kinematic sedimentation model when $u \le u_c$, where u_c is a material-dependent *critical concentration* or *gel point* at which the solid flocs start to touch each other.

It is the purpose of this paper to outline a new clarifier–thickener model for flocculated suspensions as a combination of the first-order models for ideal suspensions with the sedimentation–consolidation theory, which contributes a strongly degenerate diffusion term. The result is an initial-value problem of a strongly degenerate parabolic–hyperbolic partial differential equation, in which both the convective flux and the diffusion term depend discontinuously on x. Clearly, solutions of such an equation are in general discontinuous. The presentation of the mathematical framework in this contribution is a summary of the recent analysis [14], while the numerical examples presented herein are new and original.

To outline the present paper and put it in the proper perspective, we consider a continuously operated axisymmetric clarifier–thickener vessel as drawn in Fig. 1. Throughout this paper, we denote by x a downward increasing depth variable, and we assume that all flow variables depend on depth x and time t only. This means in particular that u is assumed to be constant across each horizontal cross-section.

We subdivide the clarifier–thickener vessel into four different zones: the thickening zone ($0 < x < x_R$), which is usually the unique zone considered in conventional analyses of continuous sedimentation, the clarification zone ($x_L < x < 0$) located above, the underflow zone ($x > x_R$) and the overflow zone ($x < x_L$). The vessel is continuously fed at depth $x = 0$, the feed level, with fresh feed suspension at a volume feed rate $Q_F(t) \ge 0$. The concentration of the feed suspension is $u_F(t)$. The prescribed volume underflow rate, at which the thickened sediment is removed from the unit, is $Q_R(t) \ge 0$. Consequently, the overflow rate is $Q_L(t) = Q_F(t) - Q_R(t)$, where we assume that the two control functions $Q_F(t)$ and $Q_R(t)$ are chosen such that $Q_F(t) > 0$. For a vessel with constant cross-sectional area S, we define the velocities $q_L(t) := Q_L(t)/S$ and $q_R(t) := Q_R(t)/S$.

Of course, the solids concentrations in the underflow and overflow cannot be prescribed, and are part of the solution. Furthermore, we distinguish between the four abovementioned *zones* in the clarifier–thickener, which are a property of the equipment modeled, and the clear liquid, hindered settling, and compression *regions*, in which a suspension at a given point of time has the concentrations zero, $0 < u \le u_c$, and $u > u_c$, respectively. Thus, the time-dependent location of the regions is a property of a particular flow, that is, of the solution to the problem. Note that the compression region is not confined to the thickening zone. These notions are stated to emphasize that the model includes two different stationary modes of operation that are usually distinguished in the applicative literature [19]: *conventional operation*, as shown in Fig. 1(a), when the sediment level (where $u = u_c$) is located below the feed level, and *high-rate* (also known as *high-capacity*) operation, when the feed suspension is pumped into the sediment, as seen in Fig. 1(b). The second case can be produced by letting the sediment level (and thus the compression region) rise into the clarification zone. In the latter mode of operation, practitioners observe that the concentration above the compression region usually is zero. These distinctions are made in engineering applications, and we will show that both modes are captured by the model which we analyze in this paper.

In any circumstance we consider a submerged feed source at a fixed vertical location. The notion “high rate” stems from the experimentally confirmed observation that this mode of

operation usually permits higher solids throughput than the conventional, since the clarification zone can handle part of the solids feed flux. Capacity and design calculations based on the new model are, however, outside the scope of this paper. For sake of simplicity, we also neglect the action of the rake provided in most industrial thickeners, which rotates above the gently sloped floor of the thickener to move the concentrated sediment towards the discharge opening.

To put our treatment in the proper perspective, we mention that similar clarifier–thickener models were proposed by several authors including Barton et al. [20], Chancelier et al. [21] and Lev et al. [22]. All available treatments are, however, limited to the case of an ideal (non-flocculated) suspension, which is included as a special case in our analysis (when we take $\sigma_e \equiv 0$ and hence $A \equiv 0$). In addition, we point out that in [21] the problem of flux discontinuities is circumvented by smoothing out the flux around the levels $x = 0$ and $x = x_R$ (in our notation). Important contributions to the study of clarifier–thickener models for ideal suspensions have been made by Diehl [23–27]. Numerical simulations using a Godunov-type scheme are presented in [24–26]. The paper by Concha et al. [19] presents a limited discussion of steady states for a steady-state clarifier–thickener model for flocculated suspensions that has many features in common with the one presented here but is incomplete in that boundary conditions or flux transitions at the discharge level are lacking. We also mention that in a recent series of papers [8,9,11,13] the authors with collaborators have put these first-order clarifier–thickener models on a firm ground concerning rigorous mathematical and numerical analysis.

The remainder of this paper is organized as follows. In Section 2 we introduce the mathematical model for the clarifier–thickener unit. The result is an initial-value problem for second-order parabolic differential equation, which exhibits two main non-standard features: a degenerating diffusion term, which accounts for the sediment compressibility, and coefficients that are discontinuous with respect to the spatial variable. In Section 3 we describe an easily implemented finite-difference scheme for the model. The non-standard features of the model required a thorough mathematical analysis [14]. Details of this research are beyond the scope of this contribution, but Section 4 summarizes the mathematical framework for the clarifier–thickener model and results of recent analysis. In particular, it becomes clear why the scheme outlined in Section 3 can be regarded as a reliable simulation tool. A limited analysis of steady-state solutions for the clarifier–thickener model is presented in Section 5. Numerical simulations of filling up a clarifier–thickener, transitions between steady states and enforcing overflow are presented in Section 6.

It should be pointed out that due to its mathematical nature, Section 4 is somewhat more technical in language, but the remaining parts of the paper (Sections 5 and 6) are readily accessible to a general audience.

2. Mathematical model

2.1. Balance equations

Consider a vertical vessel with a constant cross-sectional area S. According to [14,28], the governing partial differential equation for the solids concentration $u = u(x, t)$ can be stated as

$$\frac{\partial u}{\partial t} + \frac{\partial}{\partial x}(q(t)u + u(1-u)v_r) = 0, \tag{2.1}$$

where $q(t)$ is the volume averaged velocity of the mixture and v_r the solid–fluid relative velocity. The kinematic sedimentation theory [7] is based on the assumption that v_r is a function of u only, $v_r = v_r(u)$. The relative velocity v_r is usually expressed in terms of the Kynch batch flux density function $b(u)$, such that

$$v_r(u) = \frac{b(u)}{u(1-u)}$$

and (2.1) takes the form

$$\frac{\partial u}{\partial t} + \frac{\partial}{\partial x}(q(t)u + b(u)) = 0. \tag{2.2}$$

The function $b(u)$ is usually assumed to be piecewise differentiable with $b(u) = 0$ for $u \le 0$ or $u \ge u_{max}$, where u_{max} is the maximum solids concentration, $b(u) > 0$ for $0 < u < u_{max}$, $b'(0) > 0$ and $b'(u_{max}) \le 0$. A typical (and the most frequently used) example is [29]

$$b(u) = \begin{cases} v_\infty u(1-u)^{\hat{C}} & \text{if } 0 < u < u_{max}, \\ 0 & \text{otherwise,} \end{cases} \tag{2.3}$$

where $\hat{C} \ge 1$ and $v_\infty > 0$ is the settling velocity of a single floc in pure fluid. However, in this paper we adopt the formula due to Vesilind [30]

$$b(u) = \begin{cases} v_\infty u \exp(-Cu) & \text{if } 0 < u < u_{max}, \\ 0 & \text{otherwise.} \end{cases} \tag{2.4}$$

For simplicity, we choose here $u_{max} = 1$.

The sedimentation–consolidation theory outlined in [15–17], which includes the sediment compressibility, leads to the equation

$$v_r = \frac{b(u)}{u(1-u)}\left(1 - \frac{\sigma_e'(u)}{\Delta\varrho g u}\frac{\partial u}{\partial x}\right), \tag{2.5}$$

where $\Delta\varrho > 0$ denotes the solid–fluid density difference, g the acceleration of gravity, and $\sigma_e(u)$ the effective solid stress function, which is now the second constitutive function (besides b) characterizing the suspension. This function is assumed to satisfy $\sigma_e(u) \ge 0$ for all u and

$$\sigma_e'(u) := \frac{d\sigma_e(u)}{du} \begin{cases} = 0 & \text{for } u \le u_c, \\ > 0 & \text{for } u > u_c. \end{cases} \tag{2.6}$$

A commonly used semi-empirical effective stress formula is the power law

$$\sigma_e(u) = \begin{cases} 0 & \text{for } u \le u_c, \\ \sigma_0((u/u_c)^k - 1) & \text{for } u > u_c \end{cases} \tag{2.7}$$

with parameters $\sigma_0 > 0$ and $k > 1$. Note that the derivative $\sigma_e'(u)$ of the function defined in (2.7) is in general discontinuous at $u = u_c$. Inserting (2.5) into (2.1) and defining

$$a(u) := \frac{b(u)\sigma_e'(u)}{\Delta\varrho g u}, \qquad A(u) := \int_0^u a(s)\,\mathrm{d}s, \tag{2.8}$$

we obtain the governing equation

$$\frac{\partial u}{\partial t} + \frac{\partial}{\partial x}(q(t)u + b(u)) = \frac{\partial^2 A(u)}{\partial x^2}. \tag{2.9}$$

Since $a(u) = 0$ for $u \le u_c$ and $u = u_{max}$ and $a(u) > 0$ otherwise, (2.9) is first-order hyperbolic for $u \le u_c$ and second-order parabolic for $u > u_c$. Since (2.9) degenerates into hyperbolic type on a solution value interval of positive length, (2.9) is called strongly degenerate parabolic. The location of the type-change interface $u = u_c$ (the sediment level) is in general unknown beforehand.

For the determination of appropriate functions $b(u)$ and $\sigma_e(u)$ for real materials, see [28,31,32]. Moreover, the sedimentation–consolidation model is equivalent to the suspension dewatering theory employed in [33–36], and other works by the same group of authors.

Finally, we point out that combining (2.4) and (2.7), we get

$$a(u) = \begin{cases} a_0 \exp(-Cu)u^{k-1} & \text{for } u_c < u \le u_{max}, \\ 0 & \text{otherwise}, \end{cases} \tag{2.10}$$

where

$$a_0 := \frac{k\sigma_0 v_\infty}{u_c^k \Delta\varrho g}. \tag{2.11}$$

Standard calculus yields the following explicit expression for $A(u)$ when k is an integer:

$$A(u) = \begin{cases} 0 & \text{for } u \le u_c, \\ \mathrm{A}(u) - \mathrm{A}(u_c) & \text{for } u_c < u < u_{max}, \\ \mathrm{A}(u_{max}) - \mathrm{A}(u_c) & \text{for } u \ge u_{max}, \end{cases} \tag{2.12}$$

where

$$\mathrm{A}(u) = -a_0 \exp(-Cu)\left(\frac{x^{k-1}}{C} + (k-1)!\sum_{l=0}^{k-2}\frac{x^l}{l!C^{k-1}}\right). \tag{2.13}$$

2.2. The clarifier–thickener model

Eq. (2.9) is the main ingredient of the thickener model studied in [28], which only includes the thickening zone and represents the feed and discharge by boundary conditions. In the present model, the volume bulk velocities are

$$q(x,t) = \begin{cases} q_R(t) & \text{for } x > 0, \\ q_L(t) & \text{for } x < 0. \end{cases}$$

This suggests employing (2.9) with $q(t) = q_R(t)$ for $0 < x < x_R$ and $q(t) = q_L(t)$ for $x_L < x < 0$. Furthermore, we assume that in the overflow and underflow zones, the solid material is transported with the same velocity as the liquid. This means that the relative velocity between the phases vanishes, $v_r = 0$.

The feed mechanism is introduced by adding a singular source term, which we may express in terms of the derivative of the Heaviside function.

Combining these ingredients (see [14] for details), we obtain the strongly degenerate convection–diffusion problem

$$\frac{\partial u}{\partial t} + \frac{\partial}{\partial x}g(x,u) = \frac{\partial}{\partial x}\left(\gamma_1(x)\frac{\partial A(u)}{\partial x}\right), \qquad -\infty < x < \infty, \quad t > 0, \tag{2.14}$$

$$u(x,0) = u_0(x), \quad -\infty < x < \infty, \tag{2.15}$$

$$g(x,u) := \begin{cases} q_L(u - u_F) & \text{for } x < x_L, \\ q_L(u - u_F) + b(u) & \text{for } x_L < x < 0, \\ q_R(u - u_F) + b(u) & \text{for } 0 < x < x_R, \\ q_R(u - u_F) & \text{for } u > x_R. \end{cases} \tag{2.16}$$

Finally, we define the vector of discontinuity parameters $\gamma := (\gamma_1, \gamma_2)$ with

$$\gamma_1(x) := \begin{cases} 1 & \text{for } x \in (x_L, x_R), \\ 0 & \text{for } x \notin (x_L, x_R), \end{cases}$$

$$\gamma_2(w) := \begin{cases} q_L & \text{for } x < 0, \\ q_R & \text{for } x > 0 \end{cases}$$

and the flux function

$$f(\gamma(x), v) := g(x,u) = \gamma_1(x)b(u) + \gamma_2(x)(u - u_F). \tag{2.17}$$

The alternative model with varying cross-sectional area is studied in [14].

For the function $b(u)$ given by (2.4) with $v_\infty = 10^{-4}$ m/s and $C = 6$, the velocities in the clarifier–thickener $q_L = -5.0 \times 10^{-5}$ m/s and $q_R = 4.0 \times 10^{-5}$ m/s and $u_F = 0.21$, the flux functions $b(u)$ and the fluxes adjacent to the discontinuities of γ near $x = x_L$, $x = 0$ and $x = x_R$ are plotted in Fig. 2. Fig. 3 displays the effective solid stress function $\sigma_e(u)$ given by (2.7) with $\sigma_0 = 50$ Pa, $u_c = 0.2$ and $k = 6$, along with its derivative $\sigma_e'(u)$, the diffusion function $a(u)$ given by (2.10), and its primitive $A(u)$ given by (2.12). These parameters, which correspond to a hypothetical material, will also be utilized in Sections 5 and 6.

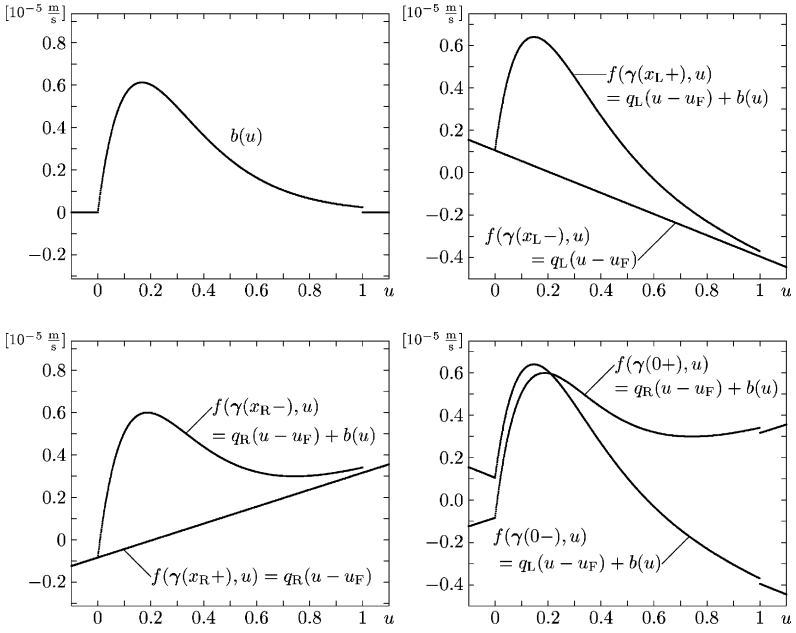

Fig. 2. The Kynch batch flux density function $b(u)$ (top left) and the fluxes adjacent to $x = x_L$ (top right), $x = x_R$ (bottom left) and $x = 0$ (bottom right).

3. Numerical scheme

The numerical scheme for the solution of (2.14)–(2.16) is a straightforward extension of the scheme used in [11] for the first-order variant of (2.14) for ideal suspensions. To define it, choose $\Delta x > 0$, set $x_j := j\Delta x$, and discretize the parameter vector γ and the initial datum by

$$\gamma_{j+1/2} := \gamma(x_{j+1/2}), \qquad U_j^0 := u_0(x_j), \quad j = 0, \pm 1, \pm 2, \ldots,$$

where $x_{j+1/2} := x_j + \Delta x/2$. In contrast to [13], we discretize u_0 and γ in a pointwise manner, rather than via cell averages, which turned out to facilitate the mathematical analysis [14]. For $n > 0$ we define the approximations according to the explicit marching formula

$$U_j^{n+1} = U_j^n - \lambda \Delta_- h(\gamma_{j+1/2}, U_{j+1}^n, U_j^n) + \frac{\lambda}{\Delta x} \Delta_- (\gamma_{1,j+1/2} \Delta_+ A(U_j^n)), \quad j = 0, \pm 1, \pm 2, \ldots, \quad n = 0, 1, 2, \ldots, \tag{3.1}$$

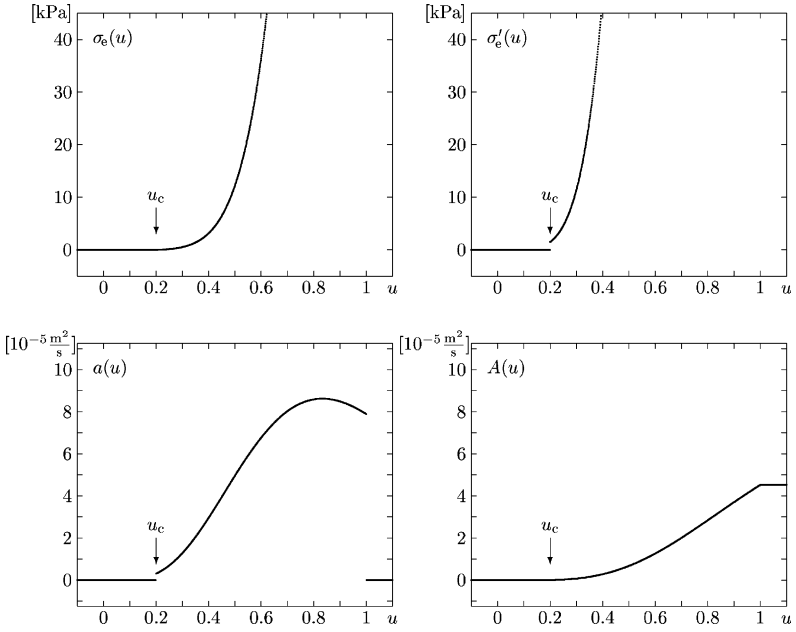

Fig. 3. The effective solid stress function $\sigma_e(u)$ (top left), its derivative $\sigma_e'(u)$ (top right), the diffusion coefficient $a(u)$ (bottom left) and its primitive $A(u)$ (bottom right).

where $\lambda := \Delta t/\Delta x$, $\Delta_- V_j := V_j - V_{j-i}$, $\Delta_+ V_j := V_{j+1} - V_j$, and

$$h(\gamma, v, u) := \frac{1}{2}\left[f(\gamma, u) + f(\gamma, v) - \int_u^v |f_u(\gamma, w)|\, \mathrm{d}w \right]$$

is the Engquist–Osher numerical flux [38]. For easy reference, we denote by u^Δ the piecewise constant function that assumes the value U_j^n on the rectangle $[x_{j-1/2}, x_{j+1/2}) \times [t_n, t_{n+1})$.

The suggested finite-difference scheme is a slightly modified version of the standard Engquist and Osher upwind scheme so that it can handle the spatial variation of the flux A key point here is that the flux parameter vector $\gamma = (\gamma_1(x), \gamma_2(x))$ is discretized on a mesh that is staggered with respect to that of the solids concentration u [39,40]. Since the discretization of γ is staggered against that of the conserved quantity u, we avoid solving the full 2×2 Riemann problem that arises at each cell boundary if the two discretizations were aligned, as in the schemes employed in [8,41].

The result is a scalar finite-difference scheme in conservation form whose flux differencing is biased in the direction of incoming waves, making it possible to resolve shocks without excessive smearing. The decisive advantage of our scheme is its simplicity.

In Section 6 we use a semi-implicit variant of (3.1) for large-time computations, in which the diffusion terms are evaluated at time t_{n+1} instead of t_n. The resulting scheme requires the solution of a system of nonlinear equations in each time step by the Newton–Raphson method. The advantage of using a semi-implicit scheme lies in the fact that we only need to satisfy a stability (CFL) condition requiring that $\Delta t/\Delta x$ is bounded, while (3.1) enforces that $\Delta t/(\Delta x)^2$ be bounded, see [14]. Thus, the semi-implicit scheme is more efficient for long-term computations, even if it involves solving a system of nonlinear equations.

4. Mathematical analysis

We start by introducing some standard notations. The classical L^p spaces of real-valued functions $u(x, t)$ are denoted by L^p, $1 \le p \le \infty$. The space BV consists of functions $u(x, t)$ of bounded variation. A locally integrable function $u(x, t)$ is an element of BV if and only if its first order distributional derivatives $\partial u/\partial x$ and $\partial u/\partial t$ can be represented by locally finite Borel measures. In this paper, we use the larger space BV_t consisting of locally integrable functions $u(x, t)$ for which only $\partial u/\partial t$ is a locally finite Borel measure. Finally, by a test function $\phi(x, t)$ we mean a compactly supported function $\phi(x, t)$ possessing continuous partial derivatives of any order.

The main ingredient in the clarifier–thickener model presented in Section 2 is the second-order strongly degenerate parabolic equation

$$\frac{\partial u}{\partial t} + \frac{\partial}{\partial x} f(\gamma(x), u) = \frac{\partial}{\partial x}\left(\gamma_1(x) \frac{\partial A(u)}{\partial x} \right), \tag{4.1}$$

where $A(u)$ is defined in (2.8) and $f(\gamma(x), u)$ is defined in (2.17). Eq. (4.1) is called strongly degenerate (or mixed hyperbolic–parabolic) because $A(u)$ has a "flat" region, which means that $A(u)$ vanishes on a solution value interval (namely, on $[0, u_c]$) of positive length.

Independently of the smoothness of $\gamma(x)$, solutions to (4.1) are in general not smooth and weak solutions must be sought, that is, integrable functions $u(x, t)$ taking values in the interval $[0, 1]$ such that $\sqrt{\gamma_1} A(u)_x \in L^2$, $u(t) \to u_0$ as $t \to 0+$ (u_0 is the prescribed initial function), and (4.1) is satisfied in the sense of distributions. However, discontinuous weak solutions are in general not uniquely determined by their initial data, so that a so-called entropy condition must be imposed to single out the physically correct solution. These "physically relevant" solutions are called entropy weak solutions. Suppose for the moment that $\gamma(x) = (\gamma_1, \gamma_2)$ is smooth.

A weak solution u is said to satisfy the *entropy condition* if for all convex twice continuously differentiable functions $\eta : \mathbb{R} \to \mathbb{R}$ there holds

$$\frac{\partial \eta(u)}{\partial t} + \frac{\partial}{\partial x} F(\gamma(x), u) + \gamma'(x) \cdot (\eta'(u) f_\gamma(\gamma(x), u) - F_\gamma(\gamma(x), u)) - \frac{\partial}{\partial x}\left(\eta'(u)\gamma_1(x) \frac{\partial A(u)}{\partial x} \right) \le 0 \tag{4.2}$$

in the sense of distributions, where the entropy flux $F(\gamma, u)$ is defined by

$$F_u(\gamma, u) = \eta'(u) f_u(\gamma, u). \tag{4.3}$$

Formally, the entropy condition (4.2) is obtained by multiplying (4.1) by $\eta'(u)$, using the chain rule, and finally discarding the term $\eta''(u)\gamma_1(x)A'(u)(\partial u/\partial x)^2$ (parabolic dissipation) thanks to the convexity of η.

By a standard approximation argument, (4.2) implies the entropy condition

$$\text{For all } c \in [0, 1]: \quad \frac{\partial}{\partial t}|u - c| + \frac{\partial}{\partial x}(\operatorname{sign}(u - c)(f(\gamma(x), u) - f(\gamma(x), c))) + \operatorname{sign}(u - c)\gamma'(x) \cdot f_\gamma(\gamma(x), c) - \frac{\partial}{\partial x}\left(\operatorname{sign}(u - c)\gamma_1(x) \frac{\partial A(u)}{\partial x} \right) \le 0$$

in the sense of distributions.

When γ is smooth, it is known that there exists a unique and stable entropy weak solution to (4.1). The mathematical theory for strongly degenerate parabolic equations (with smooth coefficients) has advanced significantly only in the last few years, and we refer to the introductory part of [14] for an overview of the relevant literature.

The very notion of entropy weak solution introduced above (in particular the entropy condition) and the corresponding well-posedness theory is not applicable when γ is discontinuous. Motivated by [42,43], in [14] we suggest a variant of the above notion of entropy weak solution that accounts for the discontinuities in γ.

Let $\mathcal{J}:=\{x_L, 0, x_R\}$ denote the set points where γ is discontinuous. For a point $m \in \mathcal{J}$, we use the notation $\gamma(m-)$ and $\gamma(m+)$ for the one-sided limits at the point m:

$$\gamma(m-):=\lim_{x\uparrow m}\gamma(x), \qquad \gamma(m+):=\lim_{x\downarrow m}\gamma(x).$$

We say that a function $u(x,t)$ is a BV_t *entropy weak solution* of the initial value problem for (4.1) if it satisfies the following conditions:

- (D.1) (regularity) $u \in L^1 \cap BV_t$, $u(x,t)$ assumes values in $[0,1]$ for all (x,t), and $A(u)_x$ is uniformly bounded on the domain $(x_L, x_R)\times(0,T)$.
- (D.2) (weak formulation) For all test functions $\phi(x,t)$

$$\int_0^T\int_{-\infty}^{\infty}\left(u\frac{\partial\phi}{\partial t}+\left[f(\gamma(x),u) -\gamma_1(x)\frac{\partial A(u)}{\partial x}\right]\frac{\partial\phi}{\partial x}\right)\mathrm{d}x\,\mathrm{d}t=0. \tag{4.4}$$

- (D.3) (initial condition) The initial condition is satisfied in the following strong sense:

$$\lim_{t\downarrow 0}\int_{-\infty}^{\infty}|u(x,t)-u_0(x)|\,\mathrm{d}x=0. \tag{4.5}$$

- (D.4) (regularity) For any $t\in[0,T]$, $x\mapsto A(u(x,t))$ is continuous at $x=x_L$ and $x=x_R$.
- (D.5) (entropy condition) The following entropy inequality holds for all $c\in[0,1]$ and all nonnegative test functions $\phi(x,t)$:

$$\int_0^T\int_{-\infty}^{\infty}\left(|u-c|\frac{\partial\phi}{\partial t}+\mathrm{sign}(u-c)\left[f(\gamma(x),u) -f(\gamma(x),c)-\gamma_1(x)\frac{\partial A(u)}{\partial x}\right]\frac{\partial\phi}{\partial x}\right)\mathrm{d}x\,\mathrm{d}t+\int_0^T\sum_{m\in\mathcal{J}} \times|f(\gamma(m+),c) -f(\gamma(m-),c)|\phi(m,t)\,\mathrm{d}t\geq 0. \tag{4.6}$$

A function $u(x,t)$ satisfying only conditions (D.1), (D.2), and (D.3) is called a BV_t *weak solution* of the initial value problem for (4.1).

Following [43], we proved in [9] that BV_t entropy weak solutions as defined above are unique and depend continuously in L^1 on their initial values. More precisely, we proved the following statement: Let v and u be two BV_t entropy weak solutions to the initial value problem for (4.1). Then for any $t\in(0,T)$

$$\int_{-\infty}^{\infty}|v(x,t)-u(x,t)|\,\mathrm{d}x\leq\int_{-\infty}^{\infty}|v(x,0)-u(x,0)|\,\mathrm{d}x. \tag{4.7}$$

Among many things, the proof of the L^1 stability (4.7), which immediately implies uniqueness, relies on jump conditions that relate limits from the right and left of the BV_t entropy weak solution u at jumps in the spatially varying coefficient $\gamma(x)$. More specifically, we use a Rankine–Hugoniot condition expressing conservation across each jump, which is a consequence of (4.4), and also an entropy jump condition, which is a consequence of (4.6).

Let u be a BV_t entropy weak solution. Fix one of the jumps in $m\in\mathcal{J}$. Then the following Rankine–Hugoniot condition holds across the jump for a.e. $t\in(0,T)$:

$$f(\gamma_+,u_+)-(\gamma_1 A(u)_x)_+=f(\gamma_-,u_-)-(\gamma_1 A(u)_x)_-,$$

where "−" denotes a spatial limit from the left and "+" denotes a spatial limit from the right. Furthermore, for $u_-(t)\neq u_+(t)$, the following entropy jump condition holds across the jump:

$$[F(\gamma_+,u_+,c)-\mathrm{sign}(u_+-c)(\gamma_1 A(u)_x)_+]-[F(\gamma_-,u_-,c) -\mathrm{sign}(u_--c)(\gamma_1 A(u)_x)_-]\leq|f(\gamma_+,c)-f(\gamma_-,c)| \quad \text{for all } c\in[0,1],$$

where $F(\gamma,u,c):=\mathrm{sign}(u-c)[f(\gamma,u)-f(\gamma,c)]$.

We mention that (D.4) is the analogue of the 'extended pressure condition' postulated in problems of multiphase flow in heterogeneous porous media (see [14] for details). These problems lead to equations with discontinuous flux and discontinuous (with respect to the space variable) diffusion, which require an additional jump condition across jumps of the diffusion coefficient (apart from the appropriate Rankine–Hugoniot condition) to ensure uniqueness. This analogy, and the observation that in our case, it seems unlikely to obtain control on the limits of $A(u)_x$ for $x\downarrow x_L$ and $x\uparrow x_R$, strongly support the postulate (D.4). Furthermore, the uniqueness proof in [14] relies on (D.4). It should be mentioned, however, that it is currently unclear how to *prove* that the numerical scheme converges to a solution that satisfies (D.4), although our numerical simulations suggest that this condition is satisfied.

In fact, in [14] we prove that the scheme converges to a limit u that satisfies all components of our definition of entropy weak solutions except (D.4). However, our numerical results support that $A(u)$ is continuous across $x=x_L$ and $x=x_R$. In particular, transient numerical simulations converge (for large times) to steady-state solutions.

In Section 3 we devised a simple explicit upwind finite-difference scheme for computing approximate BV_t entropy weak solutions. Thanks to its upwind nature, they have the built-in property that they reproduce within reasonable accuracy the discontinuities in the solutions without the necessity to track them explicitly, i.e., they are shock capturing. An obvious requirement of any numerical scheme is that it should approximate (converge to) the correct solution of the problem it is trying to solve. In the present context, this means in particular that a numerical scheme should converge as the discretization parameters tend to zero to a limit function that satisfies the entropy condition (4.6), which implies the scheme produces solutions with correct discontinuities. Under some technical conditions on the initial function u_0, it was

rigorously proved in [14] that the finite-difference scheme possessed this desired property. For the initial data, the technical conditions read

$$u_0 \in L^1((-\infty,\infty)) \cap BV((-\infty,\infty)),$$
$$u_0(x) \in [0,1] \forall x \in (-\infty,\infty),$$
$$A(u_0) \text{ is absolutely continuous on } [x_L, x_R],$$
$$\gamma_1 A(u_0)_x \in BV((-\infty,\infty)). \tag{4.8}$$

The conditions in (4.8) require that any jump in u_0 must be contained within the interval where A is constant. Let $u\Delta(x,t)$ be the piecewise constant approximate solutions defined in Section 3. In [14] we prove the following statements: There exists a BV_t weak solution of the initial value problem (4.1) that satisfies the entropy condition (D.5). With the discretization parameters Δx and Δt chosen so that the CFL condition holds, there exists a subsequence of u^Δ that converges to a limit u in $L^1((a,b)\times(0,T))$ for any pair of constants a, b such that $a<b$. Moreover, the limit function u is a BV_t weak solution of (4.1).

5. Steady-state solutions

The construction of steady states is based on the stationary version of (2.14). We do not present here a thorough analysis of all steady states but identify some stationary solutions in order to motivate the choices of the control parameters for the transient simulations. Our construction of steady states will follow a procedure similar to that of the simpler continuous thickening models treated in [28,44]. Specifically, we fix the material model, the vessel geometry, and assume that the clarifier–thickener is to be operated at given values of Q_L, Q_F and u_F, and is supposed to produce a thickened sediment of a discharge concentration $u_D > u_c$.

A steady-state solution of the clarifier–thickener can essentially be characterized as a piecewise twice differentiable function u that satisfies the following conditions:

(a) The function $\gamma_1(x)A(u)'$ is bounded, where $' = \mathrm{d}/\mathrm{d}x$.

(b) At those points where the function u and the coefficient $\gamma(x)$ are smooth, the differential equation holds, where $g(x,u)$ is given by (2.16):

$$g(x,u)' = (\gamma_1(x)A(u)')'. \tag{5.1}$$

Wherever u or γ is discontinuous, the corresponding (Rankine–Hugoniot) jump condition is valid, where $u(x^+)$ and $u(x^-)$ refer to limits of $u(\xi)$ taken for $\xi \to x$ with $\xi > x$ and $\xi < x$, respectively:

$$f(\gamma(x^-),u(x^-)) - \gamma_1(x^-)A'(u)|_{x=x^-} = f(\gamma(x^+),u(x^+)) - \gamma_1(x^+)A'(u)|_{x=x^+}. \tag{5.2}$$

It is easy to see that this condition implies that steady-state solutions are constant for $x < x_L$ and $x > x_R$.

(c) The following entropy inequality holds for all twice differentiable test functions ϕ with compact support and all real numbers k:

$$\int_{\mathbb{R}} (\mathrm{sign}(u(\xi)-k)(f(\gamma(\xi),u(\xi)) - f(\gamma(\xi),k)) - \gamma_1(\xi)A(u)')\phi'(\xi)\,\mathrm{d}\xi + \sum_{m\in\mathcal{J}} |f(\gamma(m^+),k) - f(\gamma(m^-),k)|\phi(m) \geq 0. \tag{5.3}$$

Observe that (5.3) is a time-independent version of (4.6). Inequality (5.3) implies the following entropy jump condition:

$$\mathrm{sign}(u(x^+)-k)[f(\gamma(x^+),u(x^+)) - f(\gamma(x^+),k) - \gamma_1(x^+)A'(u)|_{x=x^+}] - \mathrm{sign}(u(x^-)-k) \times [f(\gamma(x^-),u(x^-)) - f(\gamma(x^-),k) - \gamma_1(x^-)A'(u)|_{x=x^-}] \leq |f(\gamma(x^+),k) - f(\gamma(x^-),k)| \text{ for all real numbers } k. \tag{5.4}$$

Note that the right-hand part of (5.4) is zero except for $x = x_L$, $x = 0$ and $x = x_R$.

Moreover, if we introduce the limits

$$u(x^+) := \lim_{\xi\to x,\xi>x} u(\xi), \qquad u(x^-) := \lim_{\xi\to x,\xi<x} u(\xi),$$

then one can prove that (see [14] for details)

$$A(u(x^+)) = A(u(x^-)) \text{ for all } x. \tag{5.5}$$

To construct a steady-state solution that satisfies (a)–(c), we select the discharge concentration $u_D = u(x)|_{x>x_R}$ and integrate upwards (i.e., in the direction of decreasing x) the ordinary differential equation (ODE) arising from the steady-state version of the time-dependent governing partial differential equation (2.14). In doing so, we obey jump conditions wherever necessary, and thereby establish the limitations the entropy condition imposes on the choice of control parameters. Thus, the one-sided boundary condition is

$$u(x_R^-) := \lim_{x\to x_R, x<x_R} u(x) - u_D > u_c. \tag{5.6}$$

The discussion will be limited to those cases where the compression zone does not reach the overflow level. In addition, we limit ourselves to steady-state solutions for which the overflow or effluent concentration $u_E := u(x)|_{x<x_L}$ is zero, that is, we choose the parameters u_D and u_F such that

$$Q_F u_F = (Q_R - Q_L)u_F = Q_R u_D - Q_L u_E \tag{5.7}$$

is satisfied with $u_E = 0$, or, equivalently,

$$\frac{q_R - q_L}{q_R} u_F = u_D. \tag{5.8}$$

These steady states represent either the conventional or the high-rate mode of continuous operation shown in

Fig. 1(a) and (b), respectively. For convenience, we assume that

there exists exactly one point u^* with $u_c < u^* < u_{\max}$

$$\text{such that } q_L u^* + b(u^*) = q_L u_E. \tag{5.9}$$

It should be emphasized that our steady-state problem is in general overdetermined. In fact, fixing u_D and integrating (5.1) upwards and obeying entropy and jump conditions, we will in general not achieve a solution with $u|_{x<x_L} = u_E = 0$. All profiles with $u|_{w<x_L} \neq u_E = 0$ have to be rejected as candidates for steady-state entropy solutions, since they do not satisfy the global mass balance.

To determine a steady-state entropy weak solution that satisfies the global mass balance, it is in general necessary, say, to fix u_F, choose u_D, solve (5.1), to verify whether (5.7) is satisfied with u_E replaced by $u(x_L^-)$, and to iterate this solution procedure (for example, by varying u_D) until the global mass balance (5.7) is attained. However, under the simplifying assumption (5.9), it turns out that solutions with $u_E = 0$ can easily be characterized: these are those steady-state entropy weak solutions for which the compression region is strictly contained in the container. This is the most important subclass of steady states, since they are the most desired mode of operation (see Fig. 1). Moreover, it turns out that these steady-state entropy weak solutions are strictly increasing. This means that as a consequence of the entropy principle (represented here by the inequality (5.3)), and *not* by a priori assumption, the concentration at steady state increases downwards.

5.1. Steady-state solution in the discharge zone

Before proceeding to integrate the ODE (5.1) upwards from $x = x_R$, we consider the discharge zone $x > x_R$. Since we are seeking solutions for which $A(u)$ is continuous, we conclude that

$$A(u(x_R^+)) = A(u(x_R^-)) = A(u_D)$$

and therefore $A(u(x_R^+)) = u_D$. On the other hand, from (5.1) we infer that the steady-state solution must be constant for $x > x_R$. We conclude that the solution is constant in the discharge zone, i.e.

$$u(x) = u_D \quad \text{for} \quad x > x_R.$$

5.2. Steady-state solution in the thickening zone

Now that the steady-state solution has been determined for $x > x_R$, we determine the solution for $0 \le x \le x_R$, that is, in the thickening zone. To this end, note first that as a consequence of the jump condition (5.2), the steady state solution must satisfy the condition

$$q_R u_D + b(u_D) - A(u)|_{x=x_R^+} = q_R u_D,$$

which means that

$$b(u_D) - A(u)|_{x=x_R^+} = 0. \tag{5.10}$$

Assume now that $u(x)$ is a continuously differentiable solution of the following one-sided boundary value problem, which is the subcase of (5.1) occurring for the interval $(0, x_R]$:

$$q_R(u - u_D) + b(u) - A(u)' = 0 \quad \text{for} \quad x < x_R,$$
$$u(x_R) = u_D. \tag{5.11}$$

Note that we have used (5.10) to reduce the second-order ODE (5.1) to the first-order ODE (5.11). We assume that within the thickening zone, it is possible to integrate the ODE (5.11) up to the level x_c This means that x_c denotes the sediment level, when the sediment level is located in the thickening zone (i.e., $0 < x_c < x_R$), or otherwise, if it is possible to integrate (5.11) up to the feed level $x = 0$, then $x_c = 0$.

The entropy condition (5.3) imposes an additional admissibility condition, which implies that not every solution of (5.11) is an acceptable steady state solution. More precisely, this condition imposes a restriction on the choice of q_R and u_D for a given flux density function $b(u)$. In fact, in [14] we prove that any steady-state *entropy* solution $u(x)$ of (5.11) is monotonically increasing for $x_c < x < x_R$, i.e.

$$u'(x) \ge 0 \quad \text{for} \quad x_c \le x \le x_R.$$

This statement is equivalent to the requirement

$$q_R u_D \le q_R k + b(k) \ \text{ for all } k \text{ between } u(x) \text{ and } u_D$$
$$\text{for } x_c \le x \le x_R. \tag{5.12}$$

The condition (5.12) has a useful graphical interpretation: namely, the graph of $g_R(u) = q_R u + b(u)$ must lie above the horizontal line $f = q_R u_D$ fixed by the desired operation data. This condition limits the attainable solids throughput for given material and vessel.

To proceed with the discussion, we distinguish between three cases: $x_c > 0$ (Case 1), $x_c = 0$ and $u(0^+) > u_c$ (Case 2), and $x_c = 0$ and $u(0^+) = u_c$ (Case 3).

Case 1 ($x_c > 0$). In this case, the sediment level is located strictly below the feed level. The jump condition across $x = x_c$ is

$$q_R u(x_c^-) + b(u(x_c^-)) - A(u)'|_{x=x_c^-}$$
$$= q_R u(x_c^+) + b(u(x_c^+)) - A(u)'|_{x=x_c^+}, \tag{5.13}$$

respectively. Moreover, we have that

$$A(u(x_c^-)) = A(u(x_c^+)) = A(u_c) = 0,$$

so that $0 \le u(x_c^-) \le u_c$. From (5.11) and the definition of x_c it follows that

$$q_R u(x_c^+) + b(u(x_c^+)) - A(u)'|_{x=x_c^+} = q_R u_D.$$

Inserting this into (5.13), we get

$$q_R u(x_c^-) + b(u(x_c^-)) - A(u)'|_{x=x_c^-} = q_R u_D. \tag{5.14}$$

Inserting (5.11), (5.14) and $u(x_c^+) = u_c$ into the entropy jump condition (5.4) evaluated at $x = x_c$ yields

$$\operatorname{sign}(u_c - k)(q_R u_D - q_R k - b(k)) - \operatorname{sign}(u(x_c^-) - k) \times (q_R u_D - q_R k - b(k)) \le 0 \tag{5.15}$$

for all real numbers k. If k is chosen such that $u(x_c^-) < k < u_c$, then (5.15) is reduced to

$$q_R u_D \le g_R(k) = q_R k + b(k) \text{ for all } k \text{ between } u(x_c^-) \text{ and } u_c. \tag{5.16}$$

On the other hand, from (5.12) we infer that

$$q_R u_D \le q_R u_c + b(u_c).$$

This means that at $u = u_c$, the graph of $g_R(u)$ lies above or intersects the horizontal line $f = q_R u_D$. Consequently, $u(x_c^-)$ is the largest intersection of $g_R(u)$ with the horizontal line $f = q_R u_D$ that is smaller or equal to u_c. It is not difficult to see that the steady-state solution in the interval $(x_c, 0)$ is given by the constant $u(x_c^-)$, which is uniquely constructed here.

Cases 2 and 3 ($x_c = 0$, $u(0^+) \ge u_c$). The construction of the steady-state solution in the thickening zone $(0, x_R]$ is completed. The differentiable solution profile is given by the solution of the one-sided boundary value problem (5.11).

5.3. Steady-state solution in the clarification zone

Case 1 ($x_c > 0$). At $x = 0$, the next flux discontinuity has to be dealt with. However, since the solution for $x > 0$ is a constant not exceeding u_c and since $A(u)$ is continuous across $x = 0$, we have to treat a transition between two fluxes of a hyperbolic conservation law. The determination of the entropy weak solution to this problem has been treated in several papers including [8,23–25]; see [14] for further references. The basic complication is that if the fluxes adjacent to a flux discontinuity are non-monotone, then there might be several possibilities to satisfy the jump condition if a left state is given, and an application of the entropy condition is necessary to single out the unique entropy-satisfying solution. This will in general generate a multitude of cases here, depending on the flux parameters, properties of the function b, and on which solution of the equation $q_R u + b(u) = q_D u_D$ yields the relevant state in the interval. All these cases can be handled by the recent theory of conservation laws with discontinuous flux. For simplicity, however, we limit ourselves in this paper to steady-state solutions for which the sediment level at least attains (if not exceeds) the feed level, which excludes Case 1.

Case 2 ($x_c = 0$, $u(0^+) > u_c$). The continuity of $A(u)$ as a function of x implies that $u(0^-) = u(0^+)$ if $u^+ > u_c$. Thus, we can continue to solve (5.1) in the clarification zone $x \in (x_L, 0)$. Integrating this ODE over the interval $(x, 0)$, we obtain the following one-sided boundary value problem for a first-order ODE:

$$q_L(u(x) - u(0^-)) + b(u) - b(u(0^-)) - A(u)'|_{x=0} - u'(0^-) = 0 \text{ for } x < 0, \quad u(0) = u(0^-). \tag{5.17}$$

Utilizing the jump condition (5.2) across $x = 0$ and recalling that we already know that $u(0^-) = u(0^+)$ as well as that we have been able to integrate (5.11) up to $x = 0$, we can deduce the equation

$$A(u)'|_{x=0-} = q_L u(0^-) - q_R u_D - (q_L - q_R) u_F + b(u(0^-)). \tag{5.18}$$

Finally, we insert (5.18) into (5.17), and obtain the one-sided boundary value problem

$$q_L u(x) + b(u) - A(u)' - q_R u_D - (q_L - q_R) u_F = 0, \quad x < 0, \qquad u(0) = u(0^-). \tag{5.19}$$

We now define $\tilde{x}_c$ to be the largest height (i.e., the smallest value of x) up to which it has been possible to integrate (5.19). This means that either $x_L < \tilde{x}_c < 0$ is the sediment level attained in the clarification zone, or $\tilde{x}_c = x_L$ if the sediment reaches up to the overflow level. Furthermore, we recall from (5.19) and (5.18) that we have

$$b(u(x)) - A(u)' = -q_L u(x) + q_R u_D + (q_L - q_R) u_F \quad \text{for} \quad x \in (\tilde{x}_c, 0],$$

as well as that we obtain from (5.3) the inequality

$$[\operatorname{sign}(u(0^-) - k) - \operatorname{sign}(u(x) - k)](-q_L k - b(k) + q_R u_D + (q_L - q_R) u_F) \le 0 \tag{5.20}$$

for all x between $\tilde{x}_c$ and 0 and all real numbers k.

To simplify the further discussion, we recall that $q_R u_D + (q_L - q_R) u_F = q_L u_E$. Then, the solution in the interval $(\tilde{x}_c, 0)$ in the present case is given by the solution of the one-sided boundary problem (which is a slight rearrangement of (5.19))

$$u'(x) = \frac{q_L u(x) + b(u(x)) - q_L u_E}{a(u(x))}, \quad x < 0, \qquad u(0) = u(0^-). \tag{5.21}$$

Recall that (5.9) explicitly states that there exists exactly one point u^* with $u_c < u^* < u_{max}$ such that $q_L u^* + b(u^*) = q_L u_E$.

We first assume that $u(0^+) = u(0^-) > u^*$. However, it is straightforward to show that $u(0^-) \ge u^*$ does not lead to an admissible steady-state solution, see [14] for details. The remaining case is $u(0^-) < u^*$. Then the right-hand side of the ODE in (5.21) is always positive, which implies a monotonically increasing (decreasing upwards) solution $u(x)$ until $x = \tilde{x}_c$ is reached. This solution also satisfies the entropy condition. In fact, for any $x \in (\tilde{x}_c, 0)$ with $u(x) < u(0^-)$ and for all $k \in (u(x), u(0^-))$, condition (5.20) (which is void for all other values of k and for $u(x) = u(0^-)$) implies

$2(-q_L k - b(k) + q_L u_E) \le 0$, i.e.,

$$q_L k + b(k) - q_L u_E \ge 0 \text{ for all } k \text{ between } u(x) \text{ and } u(0^-), \tag{5.22}$$

which in view of (5.21) is satisfied if $u(x)$ is a monotonically decreasing solution on $(\tilde{x}_c, 0)$.

Summarizing, we can say that in Case 2, any admissible steady-state entropy solution $u = u(x)$ with $u(0^-) = u(0^+) > u_c$ must satisfy $u(0^-) < u^*$, where u^* is the unique point between u_c and u_{max} satisfying

$$g_L(u^*) = q_L u^* + b(u^*) = q_L u_E.$$

This solution is monotonically increasing on the interval $(\tilde{x}_c, 0)$.

This conclusion also admits a graphical interpretation whenever we know the value $u(0^+) = u(0^-)$. Thus, it can be evaluated only after the solution in the thickening zone has been determined. Furthermore, combining this finding with our discussion for the thickening zone, we see that in any of the Cases 1, 2 or 3, the entropy condition and jump conditions enforce that $u'(x) \ge 0$ in the compression region.

With the present discussion, we have constructed a steady-state solution up to $\tilde{x}_c$, provided that $u(x) > u_c$ in the thickening zone. To finish the steady-state construction, let us first recall that for sake of brevity and being well aware of the incompleteness of the treatment in the present paper, we limit the discussion to those steady states for which $\tilde{x}_c > x_L$. In this case, there is a jump located at $x = \tilde{x}_c$. We now seek the constant solution value $u = u(\tilde{x}_c^-)$ in the interval $(x_L, \tilde{x}_c)$. This value must satisfy $0 \le u(\tilde{x}_c^+) \le u_c$. From the jump condition that follows from (5.2):

$$q_L u(\tilde{x}_c^-) + b(\tilde{x}_c^-) = q_L u_c + b(u_c) + A'(u)|_{x=\tilde{x}_c^+},$$

we see that the constant $u(\tilde{x}_c^-) = u_c$ is not a solution. Consequently, we look for a constant $0 \le u(\tilde{x}_c^+) < u_c$. To this end, note that the steady-state jump condition at $x = x_L$ is $g_L(u(x_L^+)) = q_L u(x_L^+) + b(u(x_L^+)) = q_L u(x_L^-) = q_L u_E$. Taking into account that $g_L(u)$ is a non-negative monotonically increasing function on $[0, u_c]$, while the right-hand side is a non-positive constant, we conclude (similar as in the discussion of Case 1) that $u_E = 0$ and $u(\tilde{x}_c^-) = 0$, i.e., the solution is zero on $(x_L, \tilde{x}_c)$.

Case 3 ($x_c = 0$, $u(0^+) = u_c$). In this case, it turns out that the solution for $x < 0$, including also the section $x < x_L$, vanishes identically, see [14] for details. Thus, the solution of Case 3 is the limiting case of Cases 1 and 2 for $u(0^+) \to u_c$.

5.4. Examples of steady states

Here and in Section 6, the flocculated suspension is characterized by the functions $b(u)$ and $\sigma_e(u)$ given by (2.4) and (2.7), respectively, with the parameters specified in Section 2, see Figs. 2 and 3. Moreover, we consider a cylindrical vessel with $x_L = -1$ m and $x_R = 1$ m.

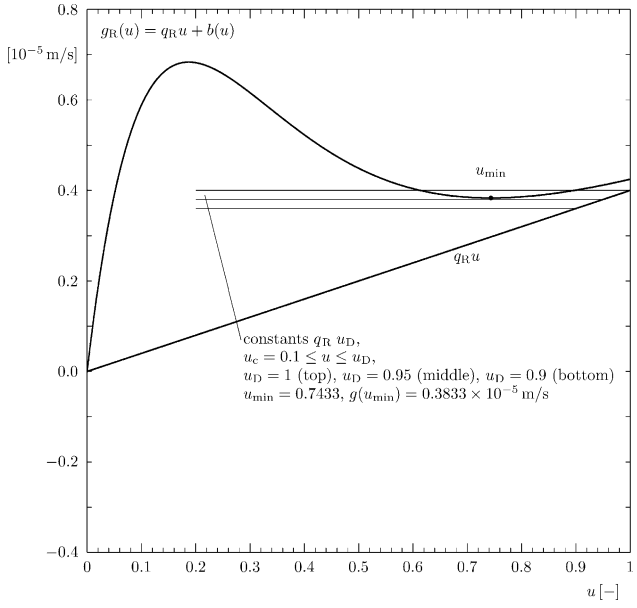

Fig. 4. The flux function $g_R(u) = q_R u + b(u)$. The plot also shows the constant lines $q_R u_D$ for some values of u_D.

As in Fig. 2, the bulk velocities $q_R = 4.0 \times 10^{-6}$ m/s and $q_L = -5.0 \times 10^{-6}$ m/s. Thus, we are interested in steady states for which

$$u_D = \frac{q_R - q_L}{q_R} u_F = 2.25 u_F$$

and these parameters have been chosen so that assumption (5.9) is satisfied. The relevant flux functions for the thickening and clarification zone, $g_R(u)$ and $g_L(u)$, are plotted in Figs. 4 and 5, respectively.

We start the steady-state construction by fixing values of u_D and limit ourselves to those values u_D that ensure that the

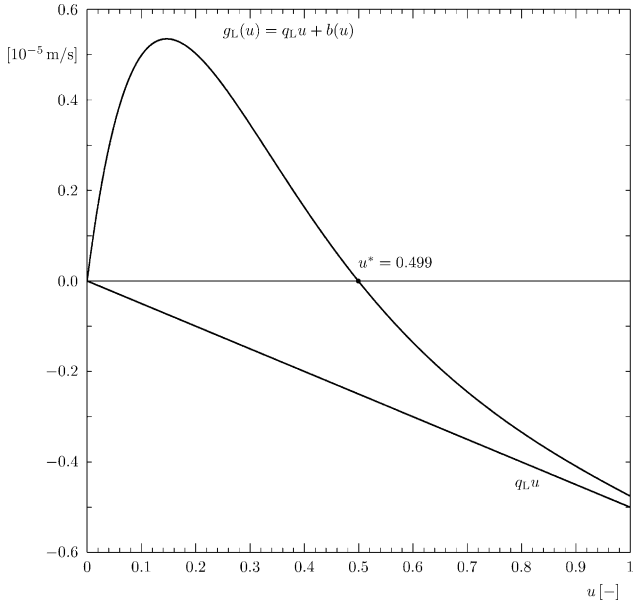

Fig. 5. The flux function $g_L(u) = q_L + b(u)$.

entropy condition (5.12) is satisfied. To this end, we consider the plot of $g_R(u)$ and draw horizontal line segments $f = q_R u_D$ for a selection of values of u_D and for $u_c \le u \le u_D$, as has been done in Fig. 4. We see that these lines remain strictly below the graph of $g_R(u)$ for those values of u_D for which

$$q_R u_D < \min_{u_c \le u \le 1} g_R(u) = g_R(0.7433) \approx 3.833 \times 10^{-6}\,\text{m/s}.$$

This implies that the entropy condition (5.12) is satisfied a priori (i.e., independently of the depth of the thickening zone x_R) for all u_D with

$$u_c \le u_D < u_{D_{max}} := \frac{1}{q_R} \min_{u_c \le u \le 1} g_R(u) = \frac{3.833 \times 10^{-6}\,\text{m/s}}{4.0 \times 10^{-6}\,\text{m/s}} = 0.9583.$$

For all other values of u_D, it would be necessary to determine a solution to (5.11), and to check whether this is monotone on $[x_c, x_R]$. Since the maximum solids concentrations attained in most real-world flocculated systems are far below 0.9583, we will not pursue this here.

Given this limitation on u_D, we choose the profiles for

$$u_F = 0.12,\ 0.13, \ldots, 0.19, 0.192, 0.193, \ldots, 0.21, 0.211, 0.215, 0.22$$

for closer inspection. Solving (5.11) with a standard numerical method for ordinary differential equations, we obtain that for $u_F \le 0.19$, we have $x_c > 0$ and therefore steady states of Case 1, while all other values lead to candidates for Case 2. Solving the equation $q_R u(x_c^-) + b(u(x_c^-)) = q_R u_D$ numerically yields the following values of $u(x_c^-)$ which we used to plot the constant concentration for the hindered settling region of the Case 1 profiles. For these values of u_D, the steady-state entropy weak solution in the clarification and overflow zones is zero. Fig. 6 includes plots of these profiles.

It remains to deal with the remaining profiles, that is, with the candidates for Case 2, for which the clarification zone has to be examined. We have just found out that all of these concentration values admit an entropy-satisfying steady-state solution in the thickening zone. For $u_D = 2.25 \times 0.215 = 0.48375$ and $u_D = 2.25 \times 0.22 = 0.495$, we obtain admissible profiles in the clarification zone, which, however, reach the overflow level $x = x_L$, and will produce an effluent with non-zero concentration u_E. These profiles are no admissible entropy steady-state solutions since the global conservation principle is violated. The values

$$u_D = 2.25 \times 0.192 = 0.43776, \ldots,$$
$$u_D = 2.25 \times 0.211 = 0.47475$$

lead to admissible steady-state profiles with $\tilde{x}_c > x_L$, and, as a consequence of our analysis, $u_E = 0$.

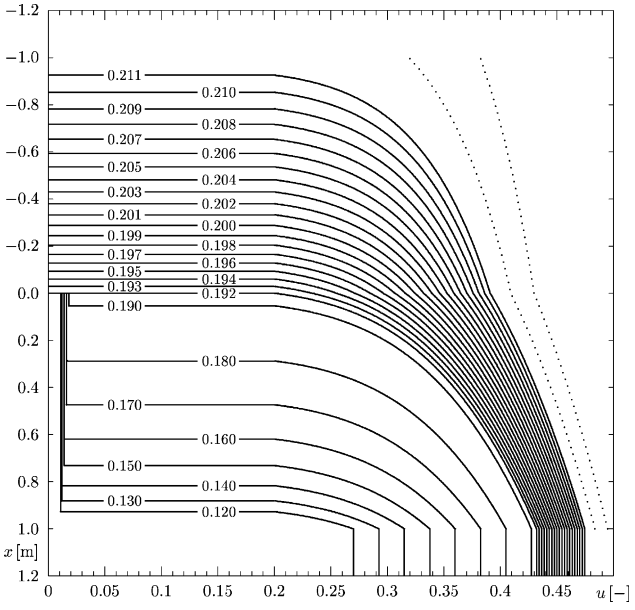

Fig. 6. Steady-state concentration profiles for the indicated values of u_F. The dotted curves show solutions of (5.11) and (5.17) that do not lead to admissible steady states with zero overflow concentration.

5.5. Concluding remark

We point out that the condition $u'(x) \ge 0$ valid for an admissible (entropy-satisfying) steady-state solution is in full agreement with engineering intuition, since one expects that in a clarifier–thickener operating properly at steady state, the concentration increases downwards. In fact, in several previous papers dealing with a simpler model of an ideal continuous thickener [28,16], which basically consists only of the thickening zone of the model discussed here, the condition $u'(x) \ge 0$ was *postulated* as a separate *requirement* for the determination of admissible steady states following just from this intuition, and the graphical condition (5.12) was derived from this condition. We now clearly see that the natural requirement that a steady state should be an entropy weak solution *implies* this monotonicity property in the thickening zone, and it is therefore *unnecessary* to introduce it as an additional condition.

Observe that in contrast to our analysis of the thickening zone, we do not apply the entropy condition to construct the restrictions on the parameters in the clarification; rather, we exploit the jump conditions to establish these restrictions, and then check that the admissible solution satisfies the entropy condition.

6. Numerical examples

In the numerical examples, we utilize the semi-implicit variant of the scheme (3.1) with $\Delta x = 0.005$ m and $\lambda = 2000$ s/m. The values of q_L and q_R are kept constant throughout, while u_F is allowed to vary as a piecewise constant function of time.

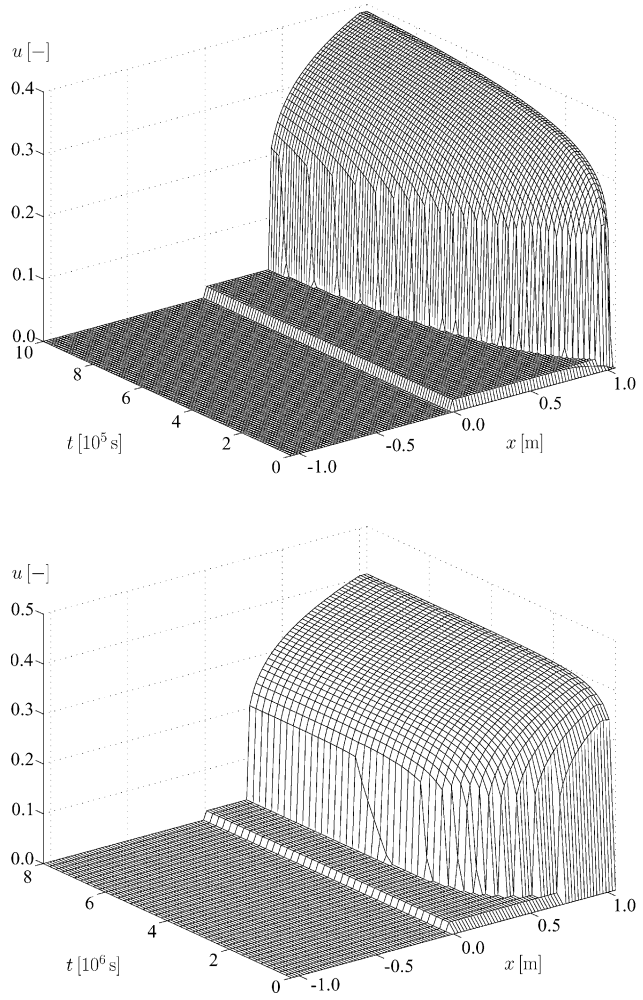

Fig. 7. Simulation of filling up a clarifier–thickener with $u_F = 0.18$: initial phase (top) and convergence to steady state (bottom).

Fig. 7 shows the simulation of filling up a clarifier–thickener that is initially full of water ($u_0 = 0$). The feed concentration is chosen as $u_F = 0.18$. The upper plot of Fig. 7 displays the initial stages of the simulation and in particular illustrates that the solids fed into the unit at the feed level exclusively pass into the thickening zone. Moreover, the concentration just above $x = x_R$ almost immediately exceeds the critical value. We observe the rise of the sediment level and the increase of the discharge concentration. The lower plot illustrates that after roughly 5.5×10^6 s (or 64 days), the system apparently attains a steady state, which seems to be the steady state of Fig. 6 corresponding to $u_F = 0.18$.

It should be commented, of course, that no plant operator would start with an empty vessel and leave it open during the fill-up process, as has been assumed here, and that by closing the equipment the fill-up can be considerably accelerated. The intention behind this and the following related examples is to demonstrate the apparent tendency of the system to converge to a stationary solution just if the operating variables (the feed concentration u_F and the bulk velocities q_L and q_R) are chosen appropriately.

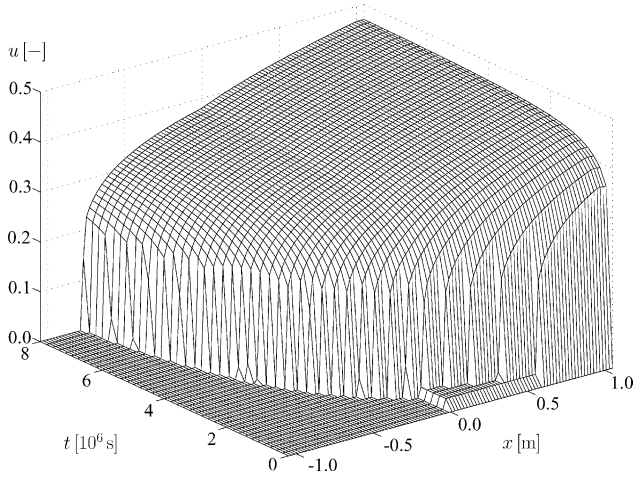

Fig. 8. Simulation of filling up a clarifier–thickener with $u_F = 0.21$.

Finally, we point out that the visual grids used in Figs. 7–11 are much coarser than the computational ones used for the numerical simulations.

Fig. 8 shows a fill-up process similar to that of Fig. 7, but with $u_F = 0.21$. Fig. 6 indicates that this value corre-

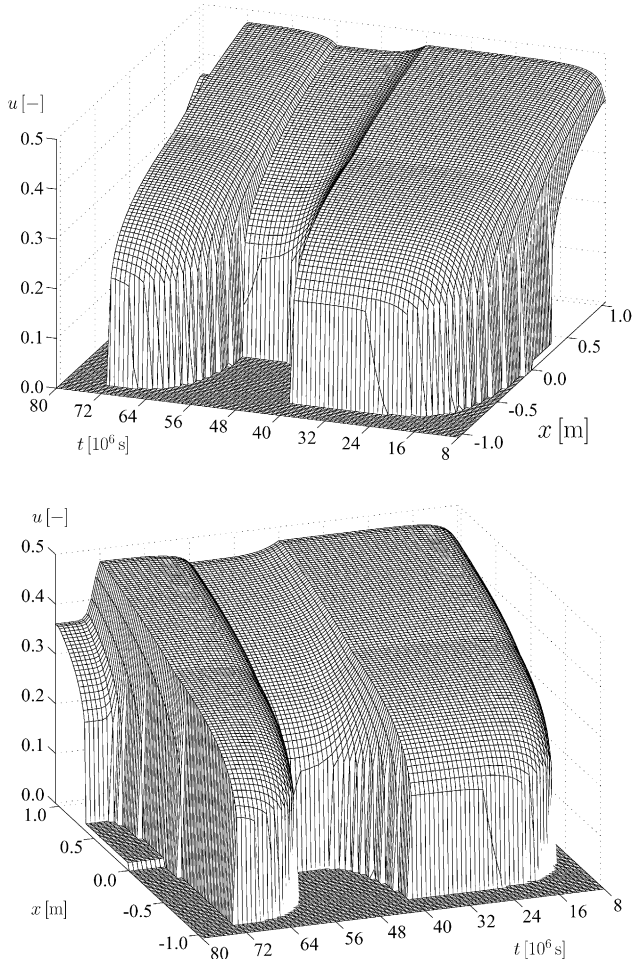

Fig. 9. Transitions between high-capacity and conventional steady states by stepwise changes of u_F (continuation of the simulation of Fig. 7).

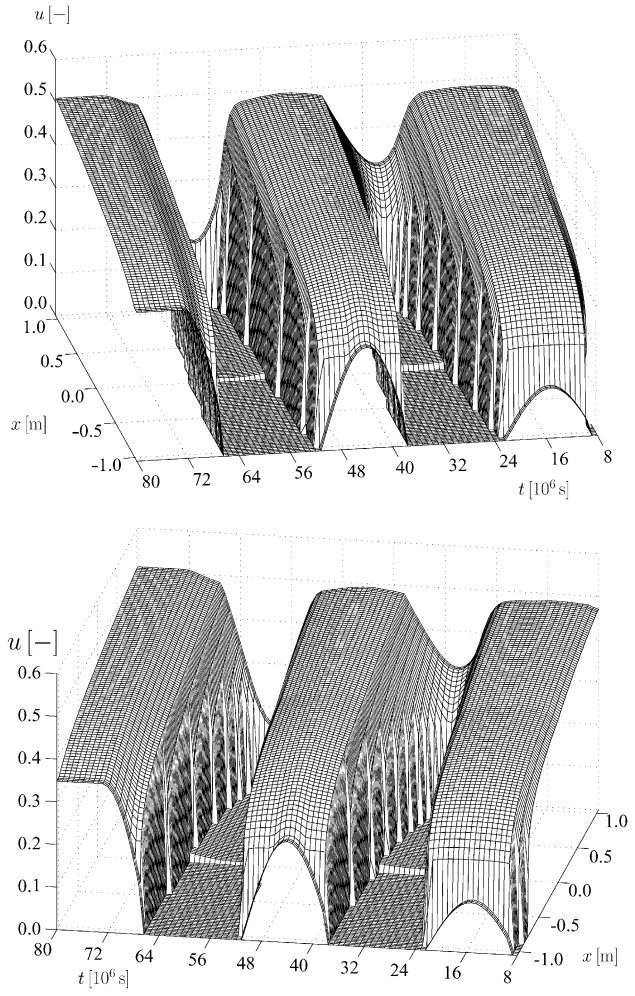

Fig. 10. Simulation of a clarifier–thickener under strongly varying feed concentration (two different views; continuation of the simulation of Fig. 8).

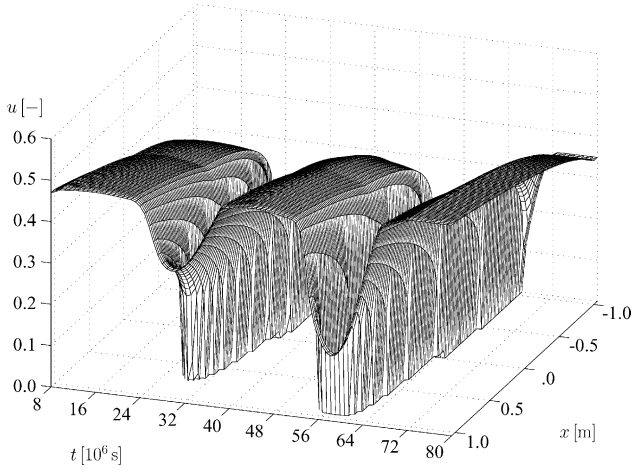

Fig. 11. A different view of the numerical simulation of Fig. 10.

sponds to a high-rate steady state, with the sediment level located in the clarification zone. Fig. 8 illustrates how the clarifier–thickener is filled up. Again, at first the feed solids settle into the thickening zone only, but the growing sediment level rapidly reaches the feed level and breaks into the clarification zone. After a simulated time of 8×10^6 s, the concentration profile is very similar to the corresponding profile shown in Fig. 6 for $u_F = 0.21$, though the numerical solution has not yet become stationary by that time.

Fig. 9 is a continuation of the simulation of Fig. 7. To illustrate the effect of the variation of the feed concentration, we change u_F in a stepwise fashion according to

$$u_F(t) = \begin{cases} 0.210 & \text{for } 8.0 \times 10^6 \text{ s} \le t < 4.0 \times 10^7 \text{ s}, \\ 0.200 & \text{for } 4.0 \times 10^7 \text{ s} \le t < 5.6 \times 10^7 \text{ s}, \\ 0.211 & \text{for } 5.6 \times 10^7 \text{ s} \le t < 7.2 \times 10^7 \text{ s}, \\ 0.16 & \text{for } t \ge 7.2 \times 10^7 \text{ s}. \end{cases} \quad (6.1)$$

Fig. 9, which consists of two different views of the same simulation, shows that the system successively assumes the steady state profiles corresponding to the values of u_F given by (6.1), see Fig. 6. Note that the location of the feed level $x = 0$ can always be traced by a faint kink in the concentration profiles. The final state of the system is the steady state of conventional operation valid for $u_F = 0.16$.

Finally, we present a continuation of the simulation of Fig. 8 produced by strongly varying the feed concentration as follows, where $T = 8.0 \times 10^7$ s:

$$u_F(t) = 0.21 + \begin{cases} 0.07 \sin(2\pi(t - 0.1T)/(0.36T)) \\ \qquad \text{for } 0.1T \le t < 0.46T, \\ 0.14 \sin(2\pi(t - 0.46T)/(0.36T)) \\ \qquad \text{for } 0.46T \le t < 0.82T, \\ 0.21 \sin(2\pi(t - 0.92T)/(0.36T)) \\ \qquad \text{for } 0.82T \le t < 0.91T, \\ 0.21 \\ \qquad \text{for } t > 0.91T. \end{cases} \quad (6.2)$$

Observe that the function $u_F(t)$ assumes values in [0, 0.42] and is continuous. Figs. 10 and 11 show three different views of the simulation of the response of the clarifier–thickener to this variation of the feed concentration. In particular, we observe how the solids break into the overflow zone. In three "waves" a non-zero effluent concentration is produced. During the first wave, however the concentration of the overflow remains below the critical value, while during the second and third wave, the critical value is exceeded. Apparently, the system eventually attains a stationary solution with non-zero overflow concentration. However, this class of steady states has for simplicity been excluded from our analysis.

Acknowledgments

This work has been supported by the Collaborative Research Center (Sonderforschungsbereich) 404 at the Univer-

sity of Stuttgart, the BeMatA program of the Research Council of Norway, and the European network HYKE, funded by the EC as contract HPRN-CT-2002-00282. RB acknowledges support by Fondecyt project 1050728 and Fondap in Applied Mathematics. The research of KHK is supported in part by an Outstanding Young Investigators Award from the Research Council of Norway.

References

[1] J.V.N. Dorr, The use of hydrometallurgical apparatus in chemical engineering, J. Ind. Eng. Chem. 7 (1915) 119–130.
[2] H.S. Coe, G.H. Clevenger, Methods for determining the capacity of slimesettling tanks, Trans. AIME 55 (1916) 356–385.
[3] R.T. Mishler, Methods for determining the capacity of slime-settling tanks, Trans. AIME 58 (1918) 102–125.
[4] R. Bürger, W.L. Wendland, Sedimentation and suspension flows: Historical perspective and some recent developments, J. Eng. Math. 41 (2001) 101–116.
[5] F. Concha, R. Bürger, A century of research in sedimentation and thickening, KONA Powder Particle 20 (2002) 38–70.
[6] F. Concha, R. Bürger, Thickening in the 20th century: a historical perspective, Miner. Metall. Process. 20 (2003) 57–67.
[7] G.J. Kynch, A theory of sedimentation, Trans. Farad. Soc. 48 (1952) 166–176.
[8] R. Bürger, K.H. Karlsen, C. Klingenberg, N.H. Risebro, A front tracking approach to a model of continuous sedimentation in ideal clarifier–thickener units, Nonlin. Anal. Real World Appl. 4 (2003) 457–481.
[9] R. Bürger, K.H. Karlsen, N.H. Risebro, A relaxation scheme for continuous sedimentation in ideal clarifier–thickener units, Comp. Math. Appl., in press.
[10] R. Bürger, K.H. Karlsen, N.H. Risebro, J.D. Towers, Numerical methods for the simulation of continuous sedimentation in ideal clarifier–thickener units, Int. J. Miner. Process. 73 (2004) 209–228.
[11] R. Bürger, K.H. Karlsen, N.H. Risebro, J.D. Towers, Monotone difference approximations for the simulation of clarifier–thickener units, Comput. Visual. Sci. 6 (2004) 83–91.
[12] R. Bürger, K.H. Karlsen, N.H. Risebro, J.D. Towers, On a model for continuous sedimentation in vessels with discontinuously varying cross-sectional area, in: T.Y. Hou, E. Tadmor (Eds.), Hyperbolic Problems: Theory, Numerics, Applications. Proceedings of the Ninth International Conference on Hyperbolic Problems held in CalTech, Pasadena, March 25–29, 2002, Springer-Verlag, Berlin, 2003, pp. 397–406.
[13] R. Bürger, K.H. Karlsen, N.H. Risebro, J.D. Towers, Well-posedness in BV_t and convergence of a difference scheme for continuous sedimentation in ideal clarifier–thickener units, Numer. Math. 97 (2004) 25–65.
[14] R. Bürger, K.H. Karlsen, J.D. Towers, A model of continuous sedimentation of flocculated suspensions in clarifier–thickener units, SIAM J. Appl. Math., in press.
[15] M.C. Bustos, F. Concha, R. Bürger, E.M. Tory, Sedimentation and Thickening, Kluwer Academic Publishers, Dordrecht, The Netherlands, 1999.
[16] R. Bürger, M.C. Bustos, F. Concha, Settling velocities of particulate systems: 9. Phenomenological theory of sedimentation processes: numerical simulation of the transient behaviour of flocculated suspensions in an ideal batch or continuous thickener, Int. J. Miner. Process. 55 (1999) 267–282.
[17] R. Bürger, W.L. Wendland, F. Concha, Model equations for gravitational sedimentation–consolidation processes, Z. Angew. Math. Mech. 80 (2000) 79–92.
[19] F. Concha, A. Barrientos, M.C. Bustos, Phenomenological model of high capacity thickening, in: Proceedings of the 19th International Mineral Processing Congress (XIX IMPC), Chapter 14, San Francisco, USA, pp. 75–79.
[20] N.G. Barton, C.-H. Li, S.J. Spencer, Control of a surface of discontinuity in continuous thickeners, J. Aust. Math. Soc. Ser. B 33 (1992) 269–289.
[21] J.P. Chancelier, M. Cohen de Lara, F. Pacard, Analysis of a conservation PDE with discontinuous flux: a model of settler, SIAM J. Appl. Math. 54 (1994) 954–995.
[22] O. Lev, E. Rubin, M. Sheintuch, Steady state analysis of a continuous clarifier–thickener system, AIChE J. 32 (1986) 1516–1525.
[23] S. Diehl, On scalar conservation laws with point source and discontinuous flux function, SIAM J. Math. Anal. 26 (1995) 1425–1451.
[24] S. Diehl, A conservation law with point source and discontinuous flux function modelling continuous sedimentation, SIAM J. Appl. Math. 56 (1996) 388–419.
[25] S. Diehl, Dynamic and steady-state behaviour of continuous sedimentation, SIAM J. Appl. Math. 57 (1997) 991–1018.
[26] S. Diehl, On boundary conditions and solutions for ideal clarifier–thickener units, Chem. Eng. J. 80 (2000) 119–133.
[27] S. Diehl, Operating charts for continuous sedimentation. I. Control of steady states, J. Eng. Math. 41 (2001) 117–144.
[28] R. Bürger, J.J.R. Damasceno, K.H. Karlsen, A mathematical model for batch and continuous thickening in vessels with varying cross-section, Int. J. Miner. Process. 73 (2004) 183–208.
[29] J.F. Richardson, W.N. Zaki, Sedimentation and fluidization, Part I, Trans. Inst. Chem. Eng. (Lond.) 32 (1954) 35–53.
[30] P.A. Vesilind, Evaluation of activated sludge thickening theories: discussion, Proc. ASCE J. Sanit. Eng. Div. 94 (1968) 185–191.
[31] R. Bürger, F. Concha, F.M. Tiller, Applications of the phenomenological theory to several published experimental cases of sedimentation processes, Chem. Eng. J. 80 (2000) 105–117.
[32] P. Garrido, R. Bürger, F. Concha, Settling velocities of particulate systems. 11. Comparison of the phenomenological sedimentation–consolidation model with published experimental results, Int. J. Miner. Process. 60 (2000) 213–227.
[33] A.A.A. Aziz, R.G. de Kretser, D.R. Dixon, P.J. Scales, The characterisation of slurry dewatering, Water Sci. Technol. 41 (8) (2000) 9–16.
[34] R.G. De Kretser, S.P. Usher, P.J. Scales, D.V. Boger, K.A. Landman, Rapid filtration measurement of dewatering design and optimization parameters, AIChE J. 47 (2001) 1758–1769.
[35] D.R. Lester, Colloidal suspension dewatering analysis, Ph.D. Thesis, Department of Chemical Engineering, University of Melbourne, Australia, 2002.
[36] S.P. Usher, R.G. De Kretser, P.J. Scales, Validation of a new filtration technique for dewaterability characterization, AIChE J. 47 (2001) 1561–1570.
[38] B. Engquist, S. Osher, One-sided difference approximations for nonlinear conservation laws, Math. Comp. 36 (1981) 321–351.
[39] J.D. Towers, Convergence of a difference scheme for conservation laws with a discontinuous flux, SIAM J. Numer. Anal. 38 (2000) 681–698.
[40] J.D. Towers, A difference scheme for conservation laws with a discontinuous flux: the nonconvex case, SIAM J. Numer. Anal. 39 (2001) 1197–1218.
[41] C. Klingenberg, N.H. Risebro, Convex conservation laws with discontinuous coefficients: existence, uniqueness and asymptotic behavior, Comm. Partial Diff. Eqns. 20 (1995) 1959–1990.

[42] K.H. Karlsen, N.H. Risebro, J.D. Towers, On an upwind difference scheme for degenerate parabolic convection–diffusion equations with a discontinuous coefficient, IMA J. Numer. Anal. 22 (2002) 623–664.
[43] K.H. Karlsen, N.H. Risebro, J.D. Towers, *L* stability for entropy solutions of nonlinear degenerate parabolic convection–diffusion equations with discontinuous coefficients, Skr. K. Nor. Vid. Selsk. (2003), 49 pp.
[44] R. Bürger, S. Evje, K.H. Karlsen, K.-A. Lie, Numerical methods for the simulation of the settling of flocculated suspensions, Chem. Eng. J. 80 (2000) 91–104.